Vasoactive intestinal peptide promotes host defense against enteric pathogens by modulating the recruitment of group 3 innate lymphoid cells

Hong Bing Yu[a,1], Hyungjun Yang[a], Joannie M. Allaire[a], Caixia Ma[a], Franziska A. Graef[a], Arthur Mortha[b], Qiaochu Liang[a], Else S. Bosman[a], Gregor S. Reid[c], James A. Waschek[d], Lisa C. Osborne[e], Harry Sokol[f,g,h], Bruce A. Vallance[a,1], and Kevan Jacobson[a,1]

[a]Division of Gastroenterology, Hepatology and Nutrition, Department of Pediatrics, The University of British Columbia, Vancouver, BC, V5Z 4H4, Canada; [b]Department of Immunology, University of Toronto, Toronto, ON, M5S 1A8, Canada; [c]Division of Oncology, Department of Pediatrics, The University of British Columbia, Vancouver, BC, V5Z 4H4, Canada; [d]The Semel Institute and Department of Psychiatry, The David Geffen School of Medicine, University of California, Los Angeles, CA 90095; [e]Department of Microbiology and Immunology, Life Sciences Institute, University of British Columbia, Vancouver, BC, V6T 1Z3, Canada; [f]Gastroenterology Department, INSERM, Centre de Recherche Saint Antoine, Sorbonne Université, Paris, F-75012, France; [g]Institut national de la recherche agronomique, Micalis Institute and AgroParisTech, Jouy en Josas, F-78350, France; and [h] Paris Center for Microbiome Medicine, Fédérations Hospitalo-universitaires, Paris, F-75012, France

Edited by Marco Colonna, Washington University in St. Louis School of Medicine, St. Louis, MO, and approved August 30, 2021 (received for review April 7, 2021)

Group 3 innate lymphoid cells (ILC3s) control the formation of intestinal lymphoid tissues and play key roles in intestinal defense. They express neuropeptide vasoactive intestinal peptide (VIP) receptor 2 (VPAC2), through which VIP modulates their function, but whether VIP exerts other effects on ILC3 remains unclear. We show that VIP promotes ILC3 recruitment to the intestine through VPAC1 independent of the microbiota or adaptive immunity. VIP is also required for postnatal formation of lymphoid tissues as well as the maintenance of local populations of retinoic acid (RA)–producing dendritic cells, with RA up-regulating gut-homing receptor CCR9 expression by ILC3s. Correspondingly, mice deficient in VIP or VPAC1 suffer a paucity of intestinal ILC3s along with impaired production of the cytokine IL-22, rendering them highly susceptible to the enteric pathogen *Citrobacter rodentium*. This heightened susceptibility to *C. rodentium* infection was ameliorated by RA supplementation, adoptive transfer of ILC3s, or by recombinant IL-22. Thus, VIP regulates the recruitment of intestinal ILC3s and formation of postnatal intestinal lymphoid tissues, offering protection against enteric pathogens.

VIP | ILC3 | enteric infection | VPAC1 | CCR9

Innate lymphoid cells (ILCs) regulate inflammation, immunity, and tissue homeostasis, particularly at mucosal barrier sites (1, 2). ILCs comprise at least three subsets, sharing similar functions with their corresponding T helper (Th) 1, 2, and 17 cell subsets. ILC3s express the transcription factor RORγt and are found largely within the gastrointestinal (GI) tract, in which they provide crucial protection against enteric pathogen infections, such as those caused by *Citrobacter rodentium* (3). They do so by fortifying the intestinal mucosa via the release of the cytokine IL-22, which promotes antimicrobial defense along with strengthening epithelial barrier function. ILC3s can be divided into two main populations. One population is the $CCR6^{+}NKp46^{-}$ ILC3s, which express CD4 heterogeneously and seed the intestine during fetal development (4, 5). They play a critical role in the development of intestinal lymphoid structures, such as cryptopatches (CPs) and lymphoid follicles (ILFs) (6). CPs are small clusters of ILC3s, whereas ILFs contain both ILC3s and B cells. The other population is $CCR6^{-}$ ILC3s, which coexpress T-bet but heterogeneously express NKp46 or NKp44 (4, 7). $CCR6^{-}$ ILC3s expand after birth, and their expansion is dependent on the expression of the ligand activated transcription factor aryl hydrocarbon receptor (AhR) (7–9). While studies have demonstrated that the development and function of ILCs is regulated by cytokines, nutrients, and their metabolites (1, 10), the molecular mechanisms regulating the accumulation and localization of ILC3s are still poorly defined.

Recent studies have shown that neurotransmitters and neuropeptides, such as neuromedin U and acetylcholine, released by tissue-resident and systemic neurons can regulate the function and numbers of ILCs during homeostasis and inflammation (11–15), representing a novel aspect of neuroimmune communication that warrants further investigation. Intriguingly, the enteric nervous system (ENS) encodes a variety of neuropeptides including vasoactive intestinal peptide (VIP) (16). VIP is known to act as an immune regulator through engaging two G protein-coupled receptors, namely VPAC1 and VPAC2 (17). Interestingly, two recent studies showed that food consumption in mice led to the transient activation of enteric VIP-expressing neurons, in close proximity to clusters of $CCR6^{+}$ ILC3s that express VPAC2. Seillet et al. showed this feeding-induced release of VIP led to a transient increase in IL-22 production by the ILC3s (18), promoting intestinal barrier function. In contrast, the study by Talbot et al. demonstrated circadian controlled release of VIP

Significance

Group 3 innate lymphoid cells enriched in the gut mediate host resistance against intestinal pathogens. Their function and development can be regulated by diverse factors, including neuropeptides secreted by the enteric nervous system. We show that the neuropeptide vasoactive intestinal peptide (VIP) promotes the recruitment of these innate lymphoid cells and other immune cells to the gut through a receptor. Mice lacking VIP or its receptor were highly susceptible to an enteric pathogen infection. Replenishing the innate lymphoid cells or their secreted products into these mice was able to partially or fully restore host resistance to the infection. Thus, the enteric nervous system, through VIP, regulates the recruitment of innate lymphoid cells to the gut, offering protection against enteric pathogens.

Author contributions: H.B.Y. designed research; H.B.Y., H.Y., J.M.A., C.M., F.A.G., Q.L., and E.S.B. performed research; G.S.R., J.A.W., and H.S. contributed new reagents/analytic tools; H.B.Y., F.A.G., A.M., J.A.W., L.C.O., H.S., B.A.V., and K.J. analyzed data; and H.B.Y., B.A.V., and K.J. wrote the paper.

The authors declare no competing interest.

This article is a PNAS Direct Submission.

Published under the PNAS license.

[1]To whom correspondence may be addressed. Email: hby@mail.ubc.ca, bvallance@cw.bc.ca, or kjacobson@cw.bc.ca.

This article contains supporting information online at https://www.pnas.org/lookup/suppl/doi:10.1073/pnas.2106634118/-/DCSupplemental.

Published October 8, 2021.

Downloaded from https://www.pnas.org by 212.129.10.242 on October 30, 2025 from IP address 212.129.10.242.

significantly decreased IL-22 production by ILC3s (19). The reason for this discrepancy remains unclear, but it could be due to other interactions between ILC3s and the ENS or the intestinal microbiota that modulate their function beyond that controlled by feeding (20). Interestingly, unlike $CCR6^+$ ILC3s, $CCR6^-$ ILC3s do not express VPAC2, and IL-22 production by these cells was not affected by VIP stimulation (19). Thus, it remains to be tested whether VIP modulates other aspects of ILC3 immunity, such as their recruitment to the GI tract, or their role in controlling susceptibility to enteric infections. It is also unclear whether VIP exerts any effects on ILC3 through the VPAC1 receptor.

We previously showed that *C. rodentium* infection triggered a prolonged and significant increase in VIP-expressing nerve fibers within the GI tract (21), a response that appears protective since the administration of exogenous VIP into wild-type (WT) mice ameliorates *C. rodentium*–induced epithelial damage. This protection was thought to reflect the ability of VIP to minimize bacteria-induced disruption of tight junction proteins located between intestinal epithelial cells (IEC) (21, 22); however, the fact that VIP regulates diverse immune responses, including Th17 and ILC3 cells, suggests that VIP may coordinate a host-protective immune–IEC dialogue. While Th17 cells are important in host defense against *C. rodentium* at later stages of infection, several recent studies have highlighted that ILC3s are critical regulators of IEC function and host survival at the early stage of infection (23, 24).

Considering the protective roles played by VIP and ILC3 during host defense against enteric pathogens like *C. rodentium*, we examined whether endogenous VIP regulated ILC3-mediated immunity during homeostasis and following infection. We found that postnatal rather than prenatal VIP signaling strongly promoted the recruitment of ILC3s (and other immune cells) to the gut by signaling through VPAC1, and this effect was independent of the intestinal microbiota or adaptive immunity. Endogenous VIP was also shown to be required to maintain the expression of the gut-homing receptor CCR9 on intestinal ILC3s by regulating the local production of retinoic acid (RA) by intestinal dendritic cells. The loss of VIP or VPAC1 thus led to dramatically reduced ILC3 recruitment to the gut, predisposing VIP-deficient ($Vip^{-/-}$) mice and VPAC1-deficient ($Vpac1^{-/-}$) mice to severe *C. rodentium* infection. Notably, this heightened susceptibility was partially reversed by RA supplementation, as well as by the adoptive transfer of ILC3s, and normalized by exogenous delivery of recombinant IL-22 (rIL-22) into $Vip^{-/-}$ mice.

Results

$Vip^{-/-}$ Mice Are Highly Susceptible to *C. rodentium* Infection. While transient activation of the VIP signaling was shown to increase host susceptibility to *C. rodentium* infection (19), short-term VIP treatment ameliorated *C. rodentium*–induced colitis in WT mice (21). These seemingly contradictory findings suggest that the in vivo role of VIP in host defense against enteric infections may be more complicated than previously thought. To address this, WT and $Vip^{-/-}$ mice were infected with the *C. rodentium* strain DBS100 (25), and their body weights and survival rates were monitored for 10 d. We saw increased VIP levels in cecal tissues starting as early as 6 h post–*C. rodentium* infection (*SI Appendix*, Fig. S1*A*), consistent with our previous observation that *C. rodentium* infection induces a significant increase in neuronal VIP density in the large intestine of mice (21). Following infection, WT mice lost less than 5% by day 10 (Fig. 1*A*). In contrast, $Vip^{-/-}$ mice lost 5% of their body weight by 3 d post-infection (dpi), and their weights continued to drop, in concert with 20 to 40% succumbing to infection between 7 and 9 dpi (Fig. 1*B*). The drastic body weight loss of $Vip^{-/-}$ mice did not reflect reduced food or water intakes (*SI Appendix*, Fig. S1*B*).

In subsequent studies, we used a streptomycin-resistant derivative strain of DBS100 (Cr) (26) or a luminescent version of this *C. rodentium* strain (Cr-lux) to more readily enumerate as well as visualize the course of infection. While Cr and Cr-lux were moderately attenuated in their ability to cause mortality in $Vip^{-/-}$ mice (as compared to DBS100), they still heavily colonized mouse intestines and caused overt intestinal pathology. We assessed the infection dynamics by in vivo imaging of Cr-lux. Substantially stronger bioluminescent signals were detected, emanating from the abdomens of $Vip^{-/-}$ mice (compared to WT mice) at 6 and 10 dpi (*SI Appendix*, Fig. S1*C*), suggesting higher intestinal *C. rodentium* burdens in these mice. Upon euthanization at 10 dpi, $Vip^{-/-}$ mice also showed increased bioluminescent signals in their large intestines (*SI Appendix*, Fig. S1 *D* and *E*). Pathogen enumeration by plating confirmed that $Vip^{-/-}$ mice carried significantly higher pathogen burdens (~10- to 30-fold) in their intestinal tissues and at systemic sites (Fig. 1*C*). We also examined *C. rodentium* localization by immunostaining for the translocated intimin receptor (Tir) that selectively labels adherent *C. rodentium* (27). The colonic tissues of WT mice showed patchy Tir staining, restricted to surface epithelial cells (Fig. 1*D* and *SI Appendix*, Fig. S1*F*). In contrast, Tir staining in the tissues of $Vip^{-/-}$ mice was spread across their entire colonic mucosa, with deep penetration into colonic crypts (indicated by white arrowheads). Macroscopically, infected $Vip^{-/-}$ mice showed significant intestinal damage (i.e., severely shrunken and inflamed ceca and shortened colons) (Fig. 1 *E* and *F*). Moreover, their colonic and cecal histology displayed extensive and severe mucosal damage, whereas WT mice showed a largely preserved epithelium, as revealed by hematoxylin and eosin (H&E) staining (Fig. 1 *G* and *H* and *SI Appendix*, Fig. S1 *G* and *H*). $Vip^{-/-}$ mice also exhibited marked inflammatory cell ($CD11b^+Gr1^+$) infiltration and heightened gene transcription of proinflammatory cytokines in colonic tissues (*SI Appendix*, Fig. S1 *I* and *J*). Similar exaggerated phenotypes were seen when using littermate $Vip^{-/-}$ mice for experiments (*SI Appendix*, Fig. S2 *A*–*C*). Moreover, $Vip^{-/+}$ mice did not show any signs of haploinsufficiency (*SI Appendix*, Fig. S2*D*), suggesting that a single copy of the *Vip* gene is sufficient for protection against *C. rodentium* infection.

The intestinal microbiota is well-known to influence host susceptibility to *C. rodentium* infection (3). While the intestinal microbiota profiles of littermates WT and $Vip^{-/+}$ mice showed only subtle differences, they were very different from those of $Vip^{-/-}$ mice (*SI Appendix*, Fig. S2 *E* and *F*). We noticed a much higher level of *Bacteroides* species in $Vip^{-/-}$ mice. Interestingly, some *Bacteroides* species are capable of exacerbating infections caused by enteric pathogens, including *C. rodentium* (28). To assess whether differences in the intestinal microbiota accounted for the hyper-susceptibility of the $Vip^{-/-}$ mice to infection, we depleted the intestinal microbiota by treating both mouse strains with a mixture of antibiotics for 2 wk before infection. Despite an almost complete depletion of intestinal microbiota in WT and littermate $Vip^{-/-}$ mice (*SI Appendix*, Fig. S2*G*), $Vip^{-/-}$ mice showed significantly higher pathogen burdens in the cecum, colon, and liver (*SI Appendix*, Fig. S2*H*). However, such differences in pathogen burdens (when treated with antibiotics) are less pronounced compared to those in mice not receiving antibiotic treatment (Fig. 1*C*), suggesting that the hyper-susceptibility of $Vip^{-/-}$ mice to *C. rodentium* infection may be partially dependent on the intestinal microbiota.

$Vip^{-/-}$ Mice Show Blunted IL-22 Signaling in Their GI Tract. IL-22 plays a central role in host defense against *C. rodentium* infection (23, 29–31). We quantified *Il-22* messenger RNA (mRNA) levels in the small intestines of infected mice, with $Vip^{-/-}$ mice showing significantly lower levels as compared to WT mice at 6 dpi (Fig. 2*A*). Furthermore, $Vip^{-/-}$ mice showed reduced gene transcription of fucosyltransferase 2 (*Fut2*), regenerating islet-derived protein 3-beta

Downloaded from https://www.pnas.org by 212.129.10.242 on October 30, 2025 from IP address 212.129.10.242.

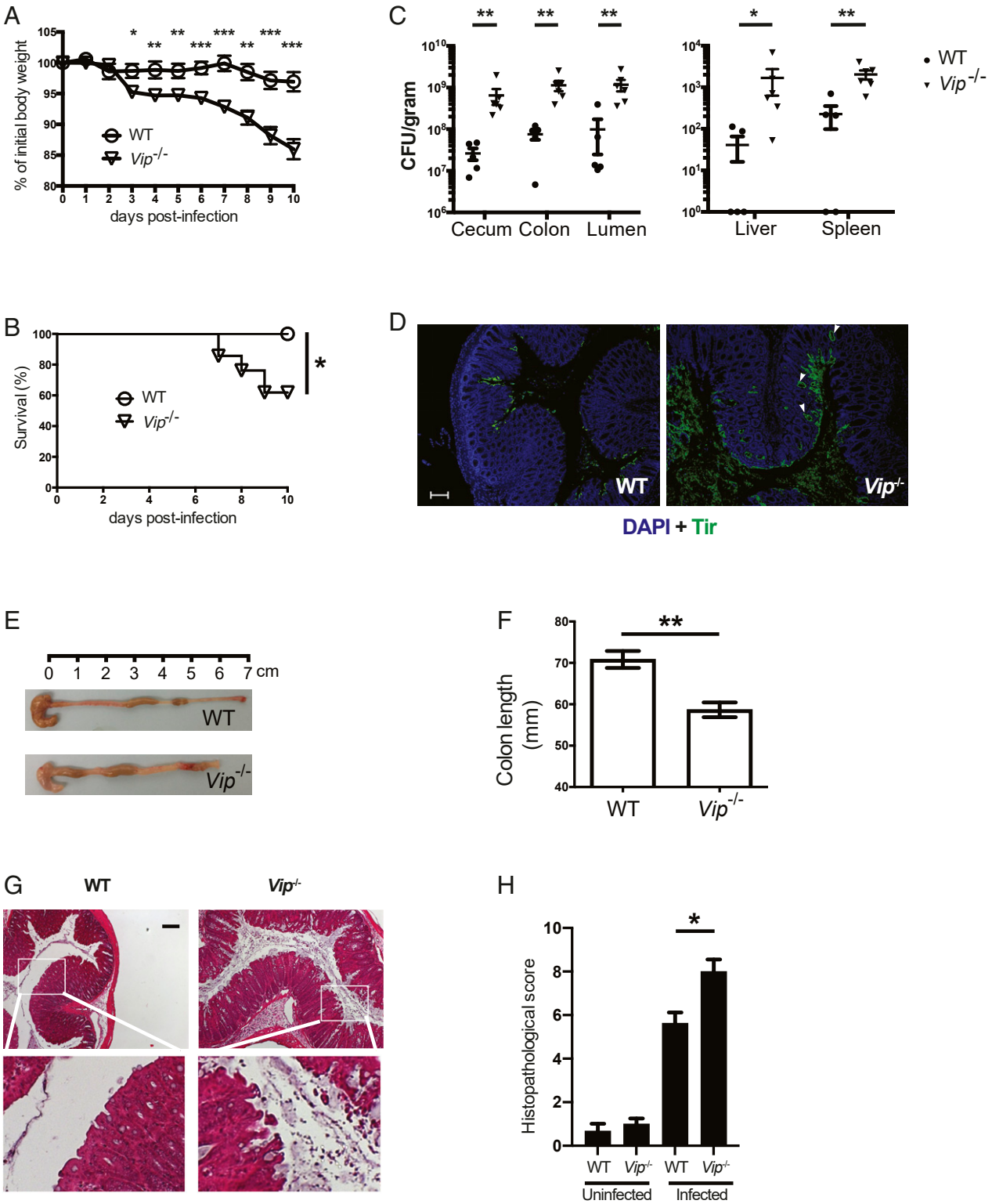

Fig. 1. *Vip*$^{-/-}$ mice are hyper-susceptible to *C. rodentium* infection. (*A* and *B*) WT ($n = 8$) and *Vip*$^{-/-}$ ($n = 10$) mice were orally infected with *C. rodentium* (DBS100, 2.5×10^8 CFU [colony-forming units]/mouse) for 10 d. Data are pooled from two independent experiments. (*A*) Body weights of infected mice are plotted as the percentage of initial (i.e., day 0) body weight. (*B*) Survival curve. (*C*–*G*) WT ($n = 5$) and *Vip*$^{-/-}$ ($n = 6$) mice were orally infected with a luminescence-expressing *C. rodentium* (Cr-lux, 2.5×10^8 CFU/mouse) for 10 d. Data are representative of two independent experiments. (*C*) Pathogen counts in indicated tissues at 10 dpi are presented. (*D*) Representative images showing *C. rodentium* (immunostained with anti-Tir, green) localization in the distal colon of WT and *Vip*$^{-/-}$ mice at 10 dpi. Host cell nuclei were stained with DAPI (blue). White arrow heads indicate deeper penetration of *C. rodentium* into the crypts. Original magnification, 200×. (Scale bar, 100 μm.) (*E*) Representative macroscopic images of large intestines at 10 dpi showing an inflamed cecum and shrunken colon in *Vip*$^{-/-}$ mice compared to WT mice. (*F*) Colons of *Vip*$^{-/-}$ mice were shorter than those of WT mice. (*G*) Representative H&E-stained distal colon sections from WT and *Vip*$^{-/-}$ mice. Boxed regions are expanded and shown in the *Bottom*. Note that *Vip*$^{-/-}$ mice show epithelial sloughing, in contrast to intact epithelium in WT mice. Original magnification, 100×. (Scale bar, 200 μm.) (*H*) Total colonic histopathological scores from WT and *Vip*$^{-/-}$ mice under uninfected ($n = 6$ for each mouse strain) and infected (10 dpi) conditions. All data are shown as mean ± SEM $^*P < 0.05$, $^{**}P < 0.01$, $^{***}P < 0.001$, by log-rank (Mantel–Cox) test (*B*) or Mann–Whitney *U* test (*A*, *C*, *F*, and *H*).

Downloaded from https://www.pnas.org by 212.129.10.242 on October 30, 2025 from IP address 212.129.10.242.

(*RegIII-β*) and *RegIII-γ*, all known to be downstream of IL-22 signaling (29, 32–34). The mRNA levels of *Il-22*, *RegIII-β*, and *RegIII-γ* were also reduced in the colons of *Vip*$^{-/-}$ mice (*SI Appendix*, Fig. S3*A*). The reduced IL-22 production in colonic tissues of *Vip*$^{-/-}$ mice was also confirmed at the protein level by enzyme-linked immunosorbent assay (*SI Appendix*, Fig. S3*B*). In addition to regulating antimicrobial responses, IL-22 is known to promote IEC proliferation (35, 36), which we assessed in colonic and ileal tissues by immunostaining for the nuclear proliferation marker Ki-67. The number of Ki-67–positive cells per colonic and ileal crypt was significantly lower in *Vip*$^{-/-}$ mice as compared to WT mice during infection (Fig. 2 *B* and *C* and *SI Appendix*, Fig. S3*C*) as well as at baseline (37). IL-22 expression is positively regulated by IL-23, another cytokine required for optimal control of *C. rodentium* infection (29, 31). Correspondingly, *Il-23* transcription was reduced in the small and large intestines of *Vip*$^{-/-}$ mice at 6 dpi (*SI Appendix*, Fig. S3*D*).

ILC3 and Th17 cells are the primary cellular sources of IL-22 (23, 29–31). To identify the cell type responsible for the blunted IL-22 responses seen in *Vip*$^{-/-}$ mice, we isolated lamina propria leukocytes (LPL) from the small (SI-LPL) and large (LI-LPL) intestines of WT and *Vip*$^{-/-}$ littermate mice. The LPL were then stimulated with PMA, ionomycin, and IL-23 and examined for IL-22 production by flow cytometry (Fig. 2*D*). The percentage and total number of IL-22-secreting linage^{-} RORγt^{+} (ILC3s) and CD3^{+}RORγt^{+} (primarily Th17 cells) in the SI-LPL were significantly reduced in *Vip*$^{-/-}$ mice as compared to WT mice (Fig. 2 *E* and *F*). Similar reductions were seen in the large intestines of *Vip*$^{-/-}$ mice (*SI Appendix*, Fig. S3 *E* and *F*). Our results also showed that the majority of IL-22–producing cells recovered from the large intestine at the early stage of infection were ILC3s (*SI Appendix*, Fig. S3*G*), confirming other studies (23, 24). Interestingly, ILC3s from *Vip*$^{-/-}$ mice retained their ability to produce IL-22, unlike ILC3s from *Ahr*$^{-/-}$ mice whose IL-22 production in response to IL-23 is known to be impaired (*SI Appendix*, Fig. S3*H*) (38). Collectively, we demonstrate blunted IL-22 signaling and reduced ILC3 (and Th17 cell) numbers in the intestines of *Vip*$^{-/-}$ mice.

IL-22 Treatment Rescues *Vip*$^{-/-}$ Mice from Severe *C. rodentium* Infection. To clarify whether the reduced IL-22 production in the intestines of *Vip*$^{-/-}$ mice might underlie their heightened susceptibility to *C. rodentium* infection, we treated *Vip*$^{-/-}$ mice with rIL-22. While infected *Vip*$^{-/-}$ mice given mouse IgG (control for rIL-22) rapidly lost weight, *Vip*$^{-/-}$ mice receiving rIL-22 treatment did not (Fig. 3*A*). Moreover, in vivo imaging revealed that rIL-22 treatment decreased pathogen colonization starting as early as day 2 pi and continuing throughout the infection (*SI Appendix*, Fig. S3*I*). Pathogen burdens in the GI tract and at systemic sites at 6 dpi were all markedly decreased upon rIL-22 treatment (Fig. 3*B*). Compared to the control group, rIL-22–treated *Vip*$^{-/-}$ mice also suffered less colonic shortening (76.75 ± 3.68 mm versus 93.6 ± 1.07 mm, $P < 0.01$), suggesting reduced inflammation. Indeed, colonic tissues from rIL-22–treated mice at 6 dpi displayed minimal signs of mucosal damage, with intact colonic epithelia and modest inflammatory cell infiltration and edema (Fig. 3 *C* and *D*). IL-22 treatment of

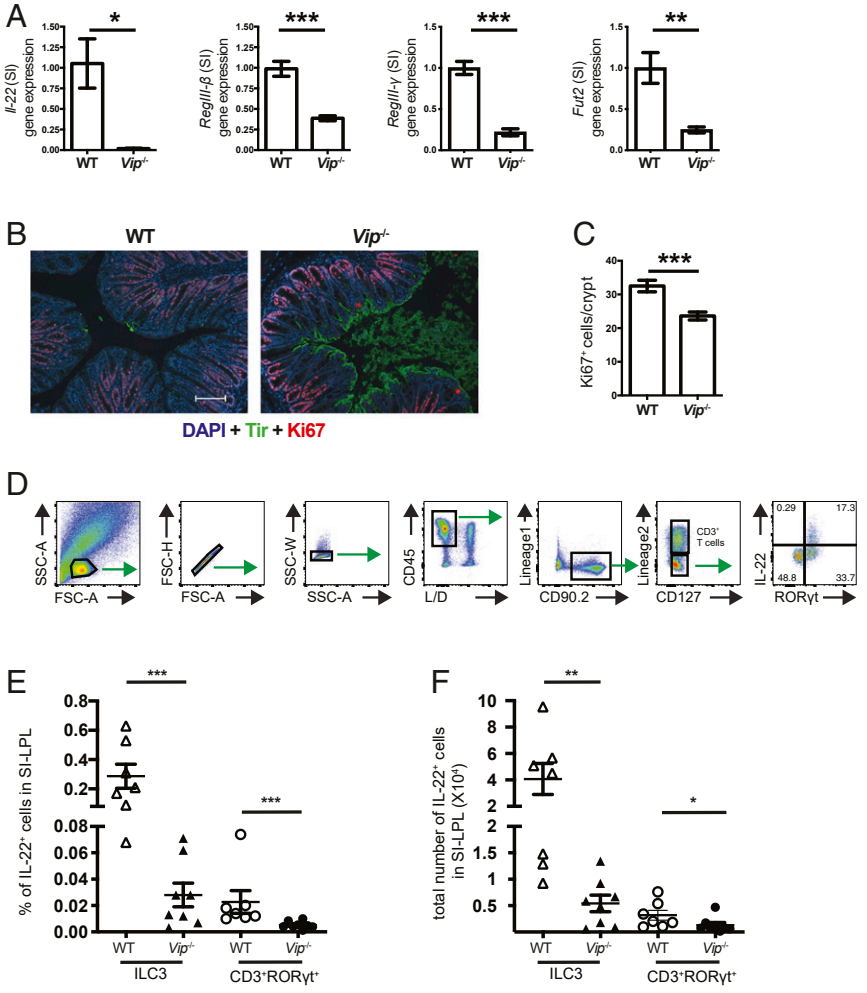

Fig. 2. *Vip*$^{-/-}$ mice show blunted IL-22 signaling in their GI tract. (*A*–*C*) WT ($n = 4$) and *Vip*$^{-/-}$ ($n = 5$) mice were orally infected with Cr (2.5×10^8 CFU/mouse) for 6 d. Data are representative of two independent experiments. (*A*) Relative gene expression of *Il-22*, *RegIII-β*, *RegIII-γ*, and *Fut2* in the small intestines (SI) of WT and *Vip*$^{-/-}$ mice. (*B*) Representative immunostaining for the proliferation marker Ki-67 (red), *C. rodentium* Tir (green), and DNA (blue) in the distal colon. Original magnification, 200×. (Scale bar, 100 μm.) (*C*) Quantification of Ki-67 positive cells/crypt in *B*. (*D*) Gating strategy for flow cytometry analysis of IL-22–secreting ILC3s and CD3^{+}RORγt^{+} (Th17s) in LPL. LPL cells were stained and gated on lymphocytes, with "doublets" excluded. L/D, live/dead cells; Lineage 1, CD11b, CD11c, and CD19; and Lineage 2, CD3ε, CD5, and CD8α. ILC3s were identified as live CD45^{+}Lin1^{-}Lin2^{-}CD127^{+}CD90.2^{+} RORγt^{+}. (*E* and *F*) SI-LPL cells from uninfected WT mice and littermate *Vip*$^{-/-}$ mice were stimulated with IL-23 (10 ng/mL), PMA (50 ng/mL), and ionomycin (1 μg/mL) for 4 h, followed by fluorescence-activated cell sorting analysis. Data are pooled from two independent experiments, and each symbol represents one mouse (*E* and *F*). Data are pooled from two independent experiments. (*E*) The percentages of IL-22^{+}ILC3s and IL-22^{+}CD3^{+}RORγt^{+} cells in SI-LPL. (*F*) Total numbers of IL-22^{+}ILC3s and IL-22^{+}CD3^{+}RORγt^{+} cells in SI-LPL. All data are shown as mean ± SEM $^{*}P < 0.05$, $^{**}P < 0.01$, $^{***}P < 0.001$, by Mann–Whitney *U* test (*A*, *C*, *E*, and *F*).

Downloaded from https://www.pnas.org by 212.129.10.242 on October 30, 2025 from IP address 212.129.10.242.

$Vip^{-/-}$ mice also led to increased transcription of *RegIII-β* and *RegIII-γ* and elevated IEC proliferation rates in the colonic mucosa (Fig. 3 *E* and *F*). These findings demonstrate that reconstitution with rIL-22 is sufficient to rescue $Vip^{-/-}$ mice from severe *C. rodentium* infection.

ILC3 Defects Underlie the Susceptibility of $Vip^{-/-}$ Mice to *C. rodentium* Infection. We next sought to identify the key cellular source (ILC3 and Th17 cells) of IL-22 that provides protection against early *C. rodentium* infection. When WT and $Vip^{-/-}$ mice were treated with a low dose of anti-CD4 mAb to transiently deplete $CD4^+$ T cells, $Vip^{-/-}$ mice were still more susceptible to infection (*SI Appendix*, Fig. S4 *A–D*). This suggests that in the absence of $CD4^+$ T cells, ILC3s may still offer protection against *C. rodentium* infection. To confirm whether it was loss of IL-22–producing ILC3 cells that increased the susceptibility of $Vip^{-/-}$ mice to infection, we sorted $CD45^{low}CD90^{high}$ ILC3s cells from the SI-LPL of $Rag1^{-/-}$ mice as described previously (23) and adoptively transferred the sorted ILC3s into $Vip^{-/-}$ mice via tail-vein injections. Curiously, despite the high number of ILC3s transferred, reconstitution in the $Vip^{-/-}$ intestine was only partial, with ILC3 numbers in the small intestine almost doubling those of the control group (phosphate-buffered saline [PBS]–treated) but still significantly lower than those in WT mice (*SI Appendix*, Fig. S4*E*). Even so, *C. rodentium*–infected $Vip^{-/-}$ mice receiving ILC3s lost less body weight and carried significantly lower pathogen burdens in their colon, spleen, and liver than the control group at 6 dpi (Fig. 3 *G* and *H*). While ILC3 transfer had little effect on gross pathology in the colons of $Vip^{-/-}$ mice (*SI Appendix*, Fig. S4*F*), it did significantly attenuate epithelial damage and improve IEC integrity scores (Fig. 3*I*). Moreover, immunostaining of colonic tissues with antibodies against Tir and actin found that in contrast to the widespread Tir staining and discontinuous/weak actin staining indicative of heavy IEC infection in the control $Vip^{-/-}$ group, mice receiving ILC3s displayed reduced Tir staining and continuous/strong actin staining (indicated by arrowhead) (Fig. 3*J*). Moreover, *Il-22* and *RegIII-γ* mRNA levels were higher in the small intestines of the ILC3 transferred $Vip^{-/-}$ mice than those in the control group (*SI Appendix*, Fig. S4*G*). These findings indicate that transplantation of ILC3s into $Vip^{-/-}$ mice partially restores protection against *C. rodentium* infection.

All ILC3 Subsets Are Decreased in the Small Intestines of $Vip^{-/-}$ Mice. Since ILC3s heterogeneously express CCR6, NKp46, T-bet, and CD4, we examined whether specific subsets of ILC3s were decreased in the absence of VIP. Using a gating strategy for intestinal $ROR\gamma t^+$ ILC3s (*SI Appendix*, Fig. S5*A*), we identified dramatically decreased numbers and percentages of all ILC3 subsets ($CCR6^+$T-$bet^-CD4^{-/+}$, $CCR6^-$T-$bet^+NKp46^{-/+}$) in the SI-LPL of $Vip^{-/-}$ mice (Fig. 4*A*). The percentage of $CCR6^-$T-bet^+ ILC3s in $Vip^{-/-}$ mice was also reduced in both $NKp46^+$ $ROR\gamma t^+$ and $NKp46^-$ $ROR\gamma t^+$ populations (*SI Appendix*, Fig. S5*B*). As intestinal $CCR6^+$ ILC3s are important for the development of CPs and ILFs, we hypothesized that loss of VIP would affect the formation of these structures in the small intestine. Immunostaining of frozen small intestines revealed both CPs ($ROR\gamma t^+$ $B220^-$) and ILFs ($ROR\gamma t^+$ $B220^+$) in WT mice, but they were almost completely lacking in littermates $Vip^{-/-}$ mice (Fig. 4 *B* and *C*). VIP also colocalized with ILC3s in the lamina propria of the small intestine (*SI Appendix*, Fig. S5*C*), confirming recent findings (18, 19). Interestingly, the loss of VIP did not affect ILC3 frequencies in mesenteric lymph nodes (MLN), spleen, or Peyer's patches (PP) (Fig. 4*D*). The numbers of PP in WT and $Vip^{-/-}$ mice were also comparable (*SI Appendix*, Fig. S5*D*). These findings suggest that VIP directs intestinal ILC3 recruitment and is required for the development of CPs and ILFs.

As described earlier, Th17 cells were reduced in $Vip^{-/-}$ mice. To determine whether other cells, such as T and B cells, mediate VIP effect on intestinal ILC3 development, we generated a $Rag1^{-/-}Vip^{-/-}$ mouse strain lacking T and B cells. Compared to $Rag1^{-/-}$ mice, $Rag1^{-/-}Vip^{-/-}$mice still showed significantly lower percentages and numbers of $ROR\gamma t^+$ ILC3s in their small intestines (Fig. 4*E*). Consistent with this, $Rag1^{-/-}Vip^{-/-}$ mice were more susceptible to *C. rodentium* infection as compared to $Rag1^{-/-}$ mice (*SI Appendix*, Fig. S5 *E–G*). Our results thus demonstrate that VIP deficiency leads to reduced number of all ILC3 subsets in the small intestine independent of the adaptive immunity.

VIP Deficiency Leads to Impaired RA Signaling and Decreased CCR9 Expression by Intestinal ILC3s. ILC3s express several homing receptors, such as CCR7, CCR9, and α4β7 (39–41), which modulate their capacity to migrate to the gut. We hypothesized that expression of these homing receptors by intestinal ILC3s might be altered in $Vip^{-/-}$ mice. As shown in Fig. 5 *A* and *B*, the expression of CCR9 was significantly lower on both $CCR6^+$ $NKp46^-$ and $CCR6^-NKp46^{-/+}$ ILC3s from the SI-LPL of $Vip^{-/-}$ mice, as compared to WT mice. Unexpectedly, while CCR9 and α4β7 expression by immune cells are often coregulated (39, 42), the expression levels of α4β7 by SI-LP ILC3s from WT and $Vip^{-/-}$ mice were comparable (*SI Appendix*, Fig. S6 *A* and *B*). The reason for this is unclear but could result from a compensatory response when endogenous VIP is missing. Further qPCR analysis revealed reduced gene expression of *Ccr9* but not *Ccl25* (whose protein product is a CCR9 ligand) in the small intestines of $Vip^{-/-}$ mice (43, 44) (Fig. 5*C*). In contrast to CCR9, CCR7 expression by $CCR6^+$ $NKp46^-$ ILC3s was significantly higher in the small intestines of $Vip^{-/-}$ mice as compared to WT mice (*SI Appendix*, Fig. S6 *C* and *D*). Thus, the loss of VIP results in reduced CCR9 expression but increased CCR7 expression by ILC3s in the small intestine.

The expression of CCR9 by intestinal ILC3s can be up-regulated in response to vitamin A and its metabolite RA (39). We analyzed vitamin A levels in the plasma and RA levels in the intestinal tissues of naïve $Vip^{-/-}$ and their WT littermate mice. Plasma vitamin A levels were slightly (albeit insignificantly) lower in $Vip^{-/-}$ mice compared to WT mice (Fig. 5*D*). In contrast, RA levels in the small intestines of $Vip^{-/-}$ mice were significantly lower than those in WT mice (Fig. 5*E*), suggesting a potential defect in the metabolism of vitamin A into RA in $Vip^{-/-}$ mice.

Intestinal $CD103^+$ DCs are one of the primary cellular sources of RA metabolized from vitamin A (39, 42, 45). We found the percentage of $CD11c^+$ DCs and $CD103^+$ $CD11c^+$ DCs in the small intestine was ∼25-fold lower in $Vip^{-/-}$ mice than in WT mice at baseline condition (Fig. 5*F*). We also noted in the SI-LPL of $Vip^{-/-}$ mice a nearly complete depletion of $CD103^+$ $CD11b^+$ $CD11c^+$ DCs (*SI Appendix*, Fig. S6*E*), the major cellular source of IL-23 (46, 47). This explains the decreased *Il-23* transcription previously seen in the small intestines of $Vip^{-/-}$ mice (*SI Appendix*, Fig. S3*C*). Moreover, the conversion of vitamin A into RA is mediated by retinaldehyde dehydrogenases, the major isoform of which is encoded by *Raldh2* and highly expressed by intestinal $CD103^+$ DCs (45, 48). As expected, the expression of *raldh2* was lower throughout the small intestine in $Vip^{-/-}$ mice compared to WT mice (*SI Appendix*, Fig. S6*F*). The reduced percentages of $CD11c^+$ DCs and $CD11c^+$ $CD103^+$ DCs were also seen in the colon, MLN, and spleen (but not PP) of $Vip^{-/-}$ mice when compared to WT mice (*SI Appendix*, Fig. S6*G*), suggesting the loss of VIP causes a general defect in DC trafficking. Despite this, $CD11c^+$ MLN cells in WT and $Vip^{-/-}$ mice displayed comparable aldehyde dehydrogenase activity (*SI Appendix*, Fig. S6*H*).

The above findings indicate that a defect in RA production is associated with decreased CCR9 expression by intestinal ILC3s in $Vip^{-/-}$ mice. We next studied whether supplementing RA

Downloaded from https://www.pnas.org by 212.129.10.242 on October 30, 2025 from IP address 212.129.10.242.

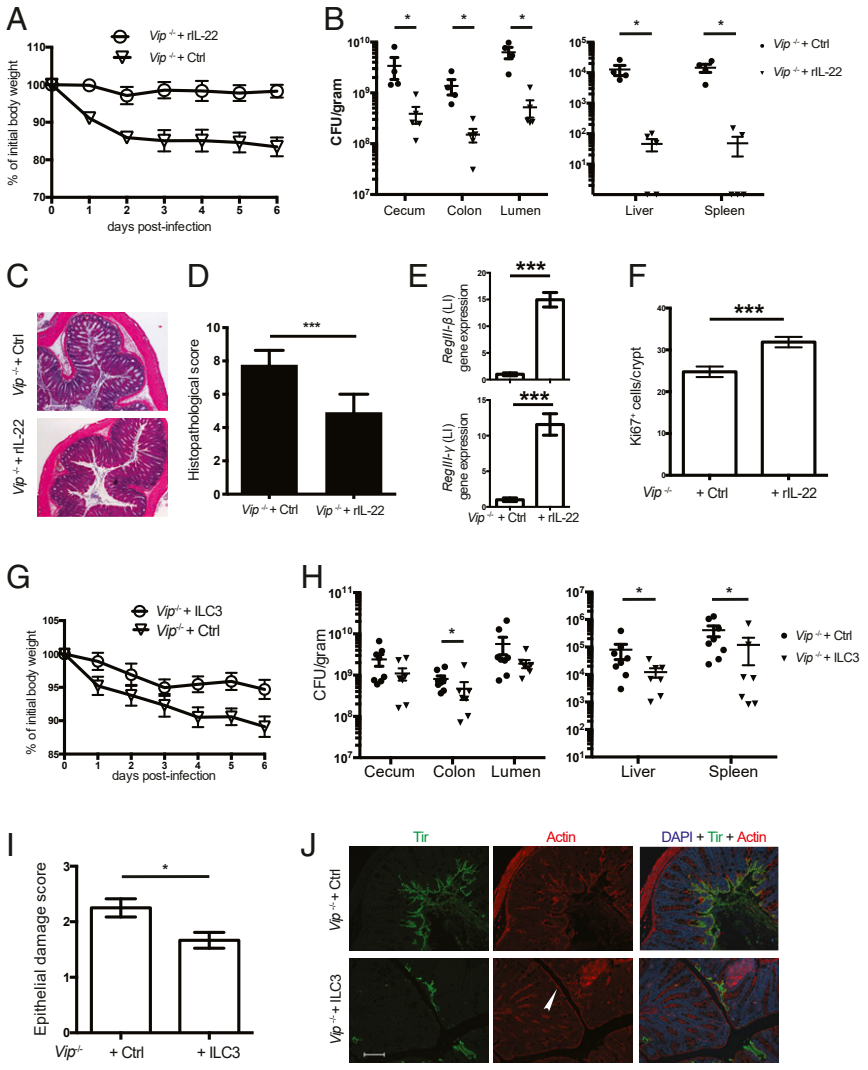

Fig. 3. ILC3 defects underlie the susceptibility of *Vip*$^{-/-}$ mice to *C. rodentium* infection. (*A–F*) IL-22 treatment rescues *Vip*$^{-/-}$ mice from *C. rodentium* infection. *Vip*$^{-/-}$ mice were injected intraperitoneally with mouse isotype IgG control ($n = 4$) or mouse IL-22-Fc protein ($n = 5$) on −5, 0, and 2 dpi (Cr-lux, 2.5 × 10^8 CFU/mouse). Data are representative of two independent experiments. (*A*) Body weights of infected mice are plotted as the percentage of initial body weight. (*B*) Pathogen counts in indicated tissues at 6 dpi are presented. (*C*) Representative H&E-stained distal colonic sections (6 dpi). Original magnification, 100×. (Scale bar, 200 μm.) (*D*) Histopathological scores from colonic tissues of WT and *Vip*$^{-/-}$ mice. (*E*) Relative gene expression of *RegIII-β* and *RegIII-γ* in the large intestines (6 dpi). (*F*) Quantification of Ki-67 positive cells/crypt at 6 dpi. (*G–J*) The lack of intestinal ILC3s underlies the hypersusceptibility of *Vip*$^{-/-}$ mice to infection. Purified ILC3s were adoptively transferred into *Vip*$^{-/-}$ mice at 0 and 2 dpi. Data are pooled from two independent experiments ($n = 8$ for WT, $n = 7$ for *Vip*$^{-/-}$). (*G*) Body weights of infected mice are plotted as the percentage of initial body weight. (*H*) Pathogen counts in indicated tissues at 6 dpi. (*I*) Colonic histopathology scores at 6 dpi. (*J*) Representative images showing the intestinal epithelial surface (stained with anti-actin, red) and localization of *C. rodentium* (stained with anti-Tir, green) in the distal colon of WT and *Vip*$^{-/-}$ mice. Host cell nuclei were stained with DAPI (blue). White arrowhead indicates a strong and continuous actin staining in WT mice, versus weak and discontinuous actin staining in *Vip*$^{-/-}$ mice. Original magnification, 200×. (Scale bar, 100 μm.) All data are shown as mean ± SEM $*P < 0.05$, $***P < 0.001$, by Mann–Whitney *U* test.

levels would restore CCR9 expression by ILC3s and normalize some of the *Vip*$^{-/-}$ mouse phenotypes. Dimethylsulfoxide (DMSO, vehicle control) or RA was injected intraperitoneally into *Vip*$^{-/-}$ mice, followed by infection with *C. rodentium*. RA supplementation led to increased CCR9$^+$ ILC3s (primarily CCR6$^+$NKp46$^-$ cells) in SI-LPL of *Vip*$^{-/-}$ mice (Fig. 5 *G* and *H*). Correspondingly, the percentage and number of RORγt$^+$ ILC3s in SI-LPL of RA-treated *Vip*$^{-/-}$ mice was almost three times that of vehicle-treated *Vip*$^{-/-}$ mice (Fig. 5*I* and *SI Appendix*, Fig. S7*A*). RA supplementation also increased IL-22 production by intestinal RORγt$^+$ ILC3s and the gene expression of *Il-22* and *RegIII-γ* in the small intestines of *Vip*$^{-/-}$ mice (*SI Appendix*, Fig. S7 *B* and *C*). Notably, RA-treated *Vip*$^{-/-}$ mice carried lower pathogen burdens in their intestinal and systemic tissues, accompanied by improved clinical symptoms (Fig. 5*J* and *SI Appendix*, Fig. S7 *D* and *E*). As a control, RA supplementation into WT mice was also found to lead to decreased pathogen loads in the cecum and liver (*SI Appendix*, Fig. S7 *F* and *G*). Taken together, our results show that the RA signaling axis is impaired in *Vip*$^{-/-}$ mice, and RA supplementation leads to increased CCR9 expression by ILC3s and ILC3 recruitment to the gut, protecting *Vip*$^{-/-}$ mice from infection.

VPAC1 Mediates the In Vivo Effect of VIP on Intestinal ILC3 Recruitment. Consistent with the reduced numbers of ILC3s seen in the SI-LPL of *Vip*$^{-/-}$ mice, the percentage of lymphocytes in these mice was dramatically reduced (Fig. 6*A*, circled populations). In contrast, *Ahr*$^{-/-}$ mice, known to have fewer intestinal ILC3s (8, 9, 38), had similar percentage of lymphocytes to that of WT mice. Interestingly, other immune cells in the SI-LPL of *Vip*$^{-/-}$ mice also showed significantly reduced numbers, although the magnitude of reduction varied (*SI Appendix*, Fig. S8*A*). This reduction appeared to be specific to the SI-LPL but not the MLN (with the exception of CD45$^+$CD3$^-$F4/80$^+$ macrophages and CD11c$^+$ DCs) (*SI Appendix*, Fig. S8*B*). These results suggest there may be a general defect in leukocyte trafficking to the intestine in *Vip*$^{-/-}$ mice, with the trafficking of lymphocytes (particularly ILC3s) being the most affected.

Many cell types, such as leukocytes, mucosal endothelium, epithelium, and stromal cells, regulate the trafficking of leukocytes to the small and large intestines (49). These cells express VPAC1 and/or VPAC2. To determine which receptor mediates the effect of VIP on promoting intestinal ILC3 recruitment, we quantified ILC3s in the SI-LPL of *Vpac1*$^{-/-}$ and *Vpac2*$^{-/-}$ mice. We also generated *Vpac1*$^{-/-}$ *Vpac2*$^{-/-}$ mice to determine whether VIP-VPAC1 and VIP-VPAC2 signaling axes acted synergistically. The percentages of lymphocytes in the SI-LPL of *Vpac1*$^{-/-}$ mice and *Vpac1*$^{-/-}$ *Vpac2*$^{-/-}$ mice but not *Vpac2*$^{-/-}$ mice were markedly lower than that of WT mice (Fig. 6*A*). As expected, *Vpac1*$^{-/-}$ mice and *Vpac1*$^{-/-}$ *Vpac2*$^{-/-}$ mice but not *Vpac2*$^{-/-}$ mice showed reduced percentages and numbers of CCR6$^+$T-bet$^-$ and CCR6$^-$T-bet$^{-/+}$

Downloaded from https://www.pnas.org by 212.129.10.242 on October 30, 2025 from IP address 212.129.10.242.

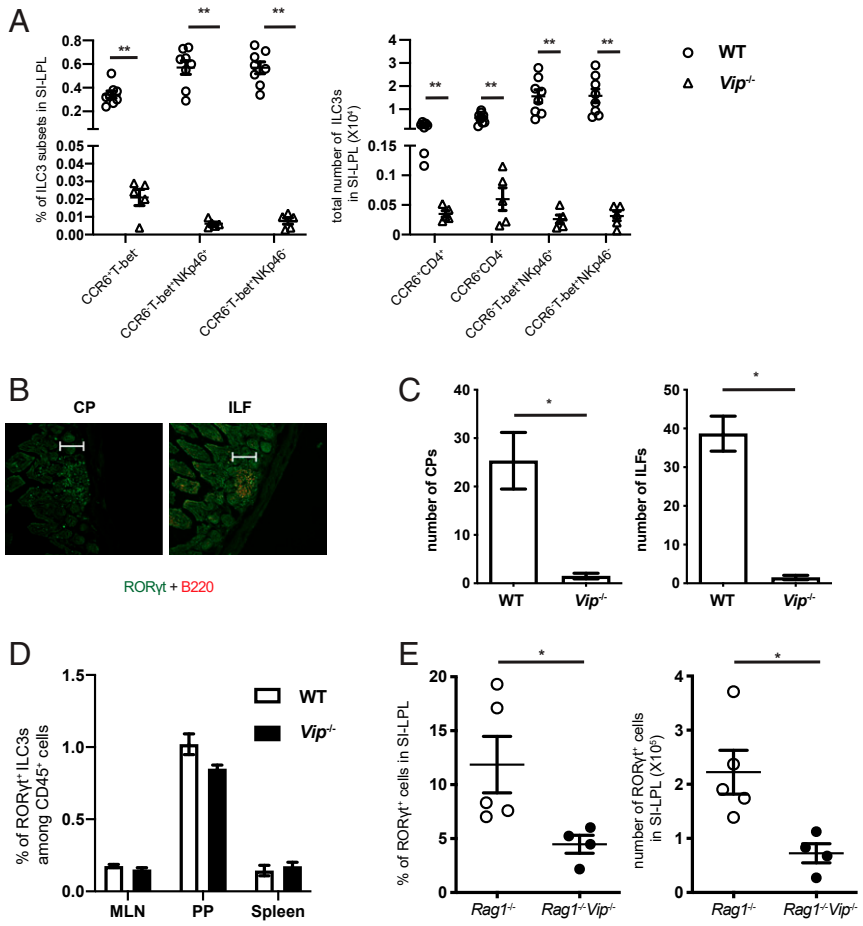

Fig. 4. All ILC3 subsets are decreased in the small intestines of *Vip*$^{-/-}$ mice. (*A*) LPL cells were isolated from the small intestines of uninfected WT (n = 8) and littermate *Vip*$^{-/-}$ mice (n = 5). Data are pooled from three independent experiments. Different ILC3 subsets were gated as in *SI Appendix*, Fig. S5*A*. The percentages (*Left*) and total numbers (*Right*) of different ILC3 subsets in SI-LPL. (*B*) Representative images of CPs and ILFs from WT mice. The small intestine tissue was stained with antibodies targeting RORγt (green) and B220 (red). Original magnification, 200×. (Scale bar, 100 μm.) (*C*) The number of CPs and ILFs in the small intestine (n = 3 for WT, n = 4 for littermate *Vip*$^{-/-}$). (*D*) The percentages of RORγt$^+$ ILC3s among CD45$^+$ cells in MLN, PP, and spleen (n = 5 for each mouse strain at baseline). (*E*) The percentages (*Left*) and total numbers (*Right*) of RORγt$^+$ ILC3s in SI-LPL of *Rag1*$^{-/-}$ and *Rag1*$^{-/-}$*Vip*$^{-/-}$ mice. Data are representative of two independent experiments (*C*–*E*). All data are shown as mean ± SEM *P < 0.05, **P < 0.01, by Mann–Whitney U test.

ILC3s in their SI-LPL as compared to their littermate WT mice (Fig. 6 *B* and *D* and *SI Appendix*, Fig. S9 *A*–*C*). These findings indicate that VPAC1 but not VPAC2 plays a role in VIP-driven recruitment of ILC3s to the gut.

Aside from ILC3s, the percentages and numbers of CD11c$^+$ DCs were significantly reduced in the SI-LPL of *Vpac1*$^{-/-}$ mice and *Vpac1*$^{-/-}$ *Vpac2*$^{-/-}$ mice, similar to that seen in *Vip*$^{-/-}$ mice (*SI Appendix*, Fig. S10 *A*–*C*). This is different from *Ahr*$^{-/-}$ mice, in which the number of CD11c$^+$ DCs was comparable to that in WT mice (*SI Appendix*, Fig. S10*D*). These data suggest that Ahr, expressed by many cell types (including ILC3s), is unlikely to mediate the effect of VIP on ILC3 recruitment.

We next explored the role of the VIP-VPAC-ILC3 axes in host defense against *C. rodentium* infection. *Vpac1*$^{-/-}$ mice, *Vpac2*$^{-/-}$ mice, and their counterpart littermates were infected with *C. rodentium* for 6 d. As shown in Fig. 6*E*, *Vpac1*$^{-/-}$ mice carried higher (10 to 100 times) intestinal and systemic pathogen burdens than their *Vpac1*$^{-/+}$ littermates. Increased pathogen burdens (4 to 20 times) were also seen in the intestines of *Vpac2*$^{-/-}$ mice as compared to *Vpac2*$^{-/+}$ mice (Fig. 6*F*). Correspondingly, both *Vpac1*$^{-/-}$ mice and *Vpac2*$^{-/-}$ mice displayed more body weight loss and increased mucosal pathology during infection (*SI Appendix*, Fig. S11 *A*–*C*). Moreover, qPCR analysis revealed significantly reduced levels of *Il-23* and *Il-22* mRNA in the ileal tissues of *Vpac1*$^{-/-}$ mice as compared to *Vpac1*$^{-/+}$ mice at 6 dpi (*SI Appendix*, Fig. S11*D*). The mRNA level of *Il-22* but not *Il-23* was also reduced in the *Vpac2*$^{-/-}$ mice. These results demonstrate that VIP promotes the recruitment of intestinal ILC3s through VPAC1 in vivo, and this VIP-VPAC1-ILC3 axis increases host resistance to *C. rodentium* infection.

VIP Acts Postnatally to Induce Intestinal ILC3 Recruitment Independent of the Intestinal Microbiota. While our observations clearly show the critical role of VIP in directing ILC3 recruitment to the intestine, it remains unclear whether VIP acts prenatally or postnatally. To address this, we examined how VIP deficiency affected the frequencies of CCR6$^+$T-bet$^-$ and CCR6$^-$T-bet$^{-/+}$ ILC3s during ontogeny. As shown in Fig. 7*A* (circled populations), the percentages of lymphocytes in the intestines of *Vip*$^{-/-}$ mice were comparable to those in WT mice at postnatal day 1 and 14 but dropped to almost 50% of WT levels by day 28. Accordingly, the frequencies of CCR6$^+$T-bet$^-$ and CCR6$^-$T-bet$^{-/+}$ ILC3s were comparable between WT and *Vip*$^{-/-}$ mice before day 14 but were significantly lower in *Vip*$^{-/-}$ mice as compared to WT mice at day 28 (Fig. 7*B*). Similar changes were also observed in other immune cells during ontogeny (*SI Appendix*, Fig. S12). These results suggest that VIP is required for the development of ILC3s (and other cell types) in the intestine after postnatal day 14. To further confirm this, we inhibited VIP signaling by treating WT mice with a VIP antagonist (VIPhyb) (50, 51). VIPhyb or PBS was intraperitoneally injected into 3- or 8-wk-old WT mice, for 3 wk. When 3-wk-old mice were used, both ILC3 subsets showed significantly reduced frequencies in SI-LPL upon VIPhyb treatment (Fig. 7*C*). In contrast, when 8-wk-old mice were used, the percentages of both ILC3s subsets were unaffected by the presence of VIPhyb.

The intestinal microbiota is known to induce a weaning reaction required for immune ontogeny (52). If the intestinal microbiota at weaning were critical for VIP-driven ILC3 recruitment to the intestine, we expected that upon the depletion of intestinal microbiota, the difference in ILC3 numbers between WT and *Vip*$^{-/-}$ mice would be diminished or abolished. WT and *Vip*$^{-/-}$ mice at the age of week 3 or 8 were thus treated with

Downloaded from https://www.pnas.org by 212.129.10.242 on October 30, 2025 from IP address 212.129.10.242.

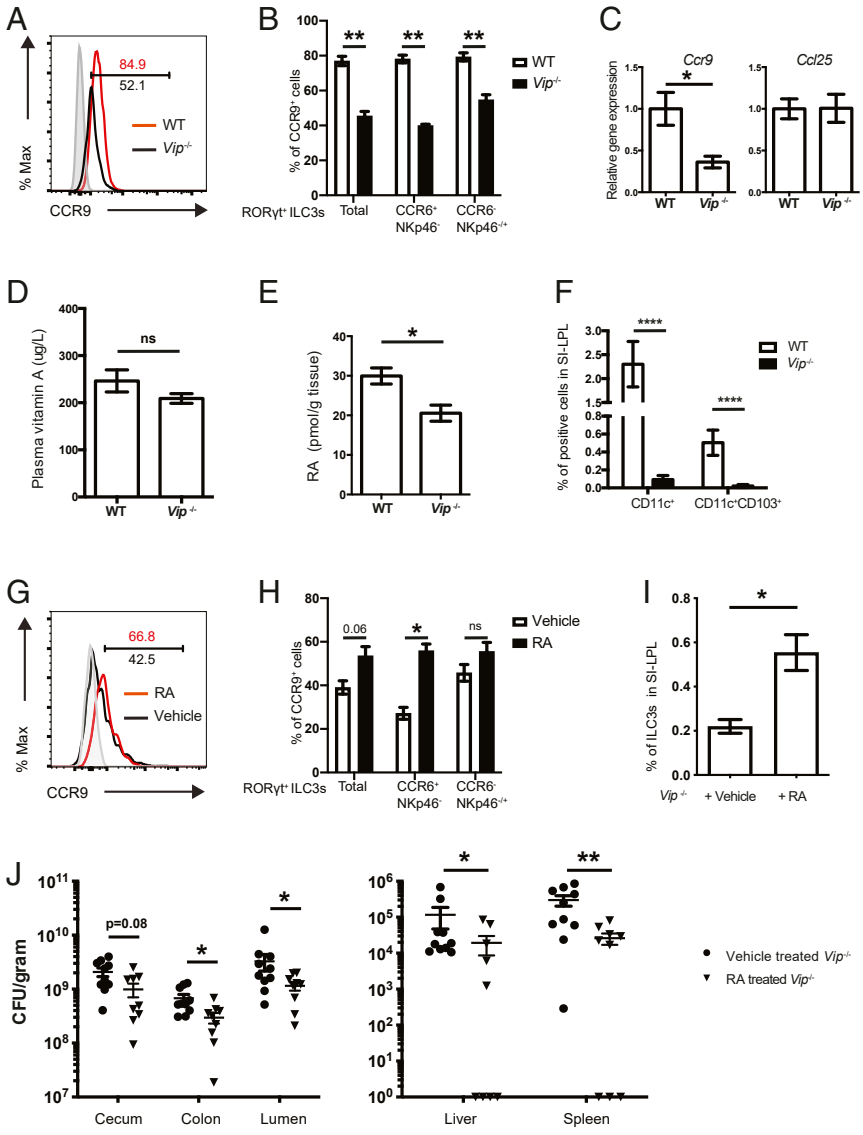

Fig. 5. VIP deficiency leads to impaired RA signaling and decreased CCR9 expression by intestinal ILC3s. (*A* and *B*) SI-LPLs from uninfected WT and littermate $Vip^{-/-}$ mice ($n = 5$ for both groups) were stained for L/D, CD45, CD90.2, Lineage 1 (CD11b/11c/19), Lineage 2 (CD3ε/5/8α), CCR6, NKp46, CD127, RORγt, and CCR9. (*A*) After gating on $Lin^{-}CD127^{+}ROR\gamma t^{+}$ cells, CCR9 expression by total ILC3s is presented as a histogram. Gray area represents fluorescence minus one (FMO) control. Data are representative of three independent experiments. (*B*) The percentages of $CCR9^{+}$ cells among total ILC3s and ILC3 subsets. (*C*) Relative gene expression of *Ccr9* and *Ccl25* in the distal ileum of uninfected WT ($n = 5$) and littermate $Vip^{-/-}$ mice ($n = 4$). Data are representative of two independent experiments. (*D*) Plasma vitamin A levels in uninfected WT ($n = 7$) and littermate $Vip^{-/-}$ mice ($n = 10$). (*E*) RA levels in the SI of uninfected WT ($n = 4$) and littermate $Vip^{-/-}$ mice ($n = 4$). (*F*) SI-LPLs from uninfected WT and littermate $Vip^{-/-}$ mice ($n = 5$ for both groups) were stained for CD45, CD103, CD11b, CD11c, and MHC-II (I-A/I-E). The percentages of $CD11c^{high}MHC\text{-}II^{high}$ and $CD103^{+}CD11c^{high}MHC\text{-}II^{high}$ in SI-LPL are presented. (*G–J*) Vehicle (DMSO) or RA was injected intraperitoneally into *C. rodentium* (2.5×10^{7} CFU/mouse) infected $Vip^{-/-}$ mice. (*G*) After gating on $Lin^{-}CD127^{+}ROR\gamma t^{+}$ cells, CCR9 expression by total ILC3s from the SI of vehicle- or RA-treated $Vip^{-/-}$ mice is presented as a histogram. Gray area represents FMO control. Data are representative of two independent experiments. (*H*) The percentages of $CCR9^{+}$ cells among total ILC3s and different ILC3 subsets from the SI of vehicle-treated $Vip^{-/-}$ ($n = 4$) and RA-treated $Vip^{-/-}$ mice ($n = 5$). (*I*) Percentage of ILC3s in SI-LPLs of vehicle- ($n = 4$) and RA-treated $Vip^{-/-}$ mice ($n = 5$). (*J*) Bacterial counts in indicated tissues of vehicle- and RA-treated $Vip^{-/-}$ mice (6 dpi). Data are pooled from two independent experiments. All data are shown as mean ± SEM $^{*}P < 0.05$, $^{**}P < 0.01$, $^{****}P < 0.0001$ by Mann–Whitney *U* test.

antibiotics for 3 wk. Surprisingly, the frequency of ILC3s in SI-LPL of $Vip^{-/-}$ mice remained significantly lower than that in WT mice, regardless of their age (Fig. 7*D*). These data suggest that the intestinal microbiota at weaning or the adult stage may play little role in VIP-driven ILC3 development in the intestine.

Together, we show that postnatal VIP signaling promotes the recruitment of intestinal ILC3s independent of the intestinal microbiota.

Discussion

The numbers and function of ILC3s are known to be regulated by exogenous signals (e.g., dietary and microbial metabolites) and endogenous signals (e.g., myeloid cell derived cytokines) (10, 53). Two recent studies demonstrated that VIP released from enteric neurons modulated the function of ILC3s through VPAC2, albeit in opposite ways (18, 19). Advancing these studies, we show that postnatal VIP signaling regulates the numbers of intestinal ILC3s through VPAC1, whereas a genetic deficiency in VIP or VPAC1 predisposes the host to enteric pathogen infections.

While $Vip^{-/-}$ mice failed to develop CPs and ILFs in their small intestinal lamina propria, they did not show any defects in the development of secondary lymphoid organs (such as MLN, spleen, and PP) or any significant changes in the frequencies of ILC3s in these organs. These observations suggest that $Vip^{-/-}$ mice do not suffer a generalized developmental and functional defect in fetal/prenatal ILC3s. Indeed, the frequencies of different subsets of ILC3s in SI-LPL were not significantly different between WT and $Vip^{-/-}$ mice until the age of week 4. Moreover, the frequency of ILC3s in SI-LPL of 3-wk-old mice was diminished upon VIPhyb treatment. This observation was not seen in VIPhyb treated 8-wk-old mice. The basis for this is unclear, but it will be interesting to determine whether prolonged treatment of adult mice with VIPhyb alters the frequency of intestinal ILC3s. Together, these findings suggest that VIP is required for the postnatal recruitment of intestinal ILC3s.

$Vip^{-/-}$ mice, starting as early as 4 wk of age, showed defective recruitment of intestinal ILC3s irrespective of their treatment with antibiotics (to deplete the intestinal microbiota), suggesting that the intestinal microbiota may not contribute to decreased intestinal ILC3s in $Vip^{-/-}$ mice. This also explains that when the intestinal microbiota were depleted, $Vip^{-/-}$ mice (as compared to WT mice) remained more susceptible to *C. rodentium* infection. Of particular interest, when the intestinal microbiota at weaning were depleted, WT mice still showed a much higher number of ILC3s (and other immune cells) as compared to $Vip^{-/-}$ mice.

Downloaded from https://www.pnas.org by 212.129.10.242 on October 30, 2025 from IP address 212.129.10.242.

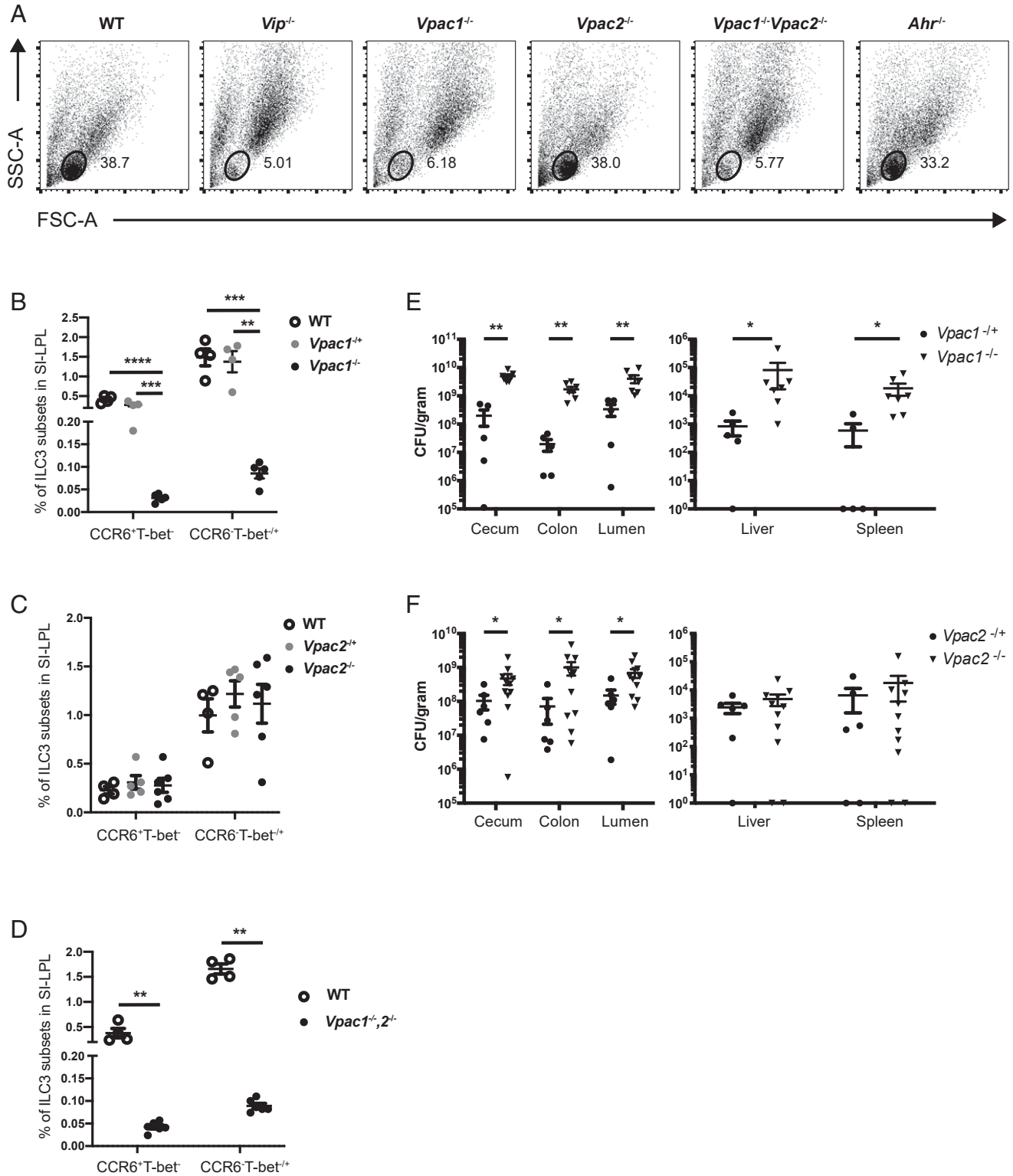

Fig. 6. VPAC1 but not VPAC2 mediates the in vivo effect of VIP on intestinal ILC3 recruitment. (*A*) SI-LPLs from uninfected WT, *Vip*$^{-/-}$, *Vpac1*$^{-/-}$, *Vpac2*$^{-/-}$, *Vpac1*$^{-/-}$*Vpac2*$^{-/-}$, and *Ahr*$^{-/-}$ mice were used for analysis. Data are representative fluorescence-activated cell sorting plots showing singlet populations. The percentages of circled populations (lymphocytes) are indicated next to the circles. (*B–D*) SI-LPLs from indicated mouse strains (uninfected) were gated as in *SI Appendix*, Fig. S9. (*B*) The percentages of different ILC3 subsets in SI-LPL of littermate WT ($n = 4$), *Vpac1*$^{-/+}$ ($n = 4$), and *Vpac1*$^{-/-}$ ($n = 5$) mice. (*C*) The percentages of different ILC3 subsets in SI-LPL of littermate WT ($n = 4$), *Vpac2*$^{-/+}$ ($n = 5$), and *Vpac2*$^{-/-}$ ($n = 6$) mice. (*D*) The percentages of different ILC3 subsets in SI-LPL of littermate WT ($n = 4$) and *Vpac1*$^{-/-}$*Vpac2*$^{-/-}$ ($n = 6$) mice. (*E* and *F*) Mice were infected with *C. rodentium* (2.5×10^7 CFU/mouse) for 6 d. (*E*) Bacterial counts in indicated tissues of littermate *Vpac1*$^{-/+}$ ($n = 5$) and *Vpac1*$^{-/-}$ ($n = 7$) mice. (*F*) Bacterial counts in indicated tissues of littermate *Vpac2*$^{-/+}$ ($n = 6$) and *Vpac2*$^{-/-}$ ($n = 11$) mice. Data are pooled from two or three independent experiments (*B–F*). All data are shown as mean ± SEM *$P < 0.05$, **$P < 0.01$, ***$P < 0.001$, ****$P < 0.0001$ by ANOVA with Tukey's test (*B*, *C*) or Mann–Whitney *U* test (*D–F*).

Downloaded from https://www.pnas.org by 212.129.10.242 on October 30, 2025 from IP address 212.129.10.242.

This is somewhat unexpected, since the intestinal microbiota at weaning plays a key role in inducing a vigorous immune reaction (52). Future generation of germ-free *Vip*$^{-/-}$ mice will conclusively define the role of the intestinal microbiota in VIP-driven ILC3 recruitment.

Similar to *Vip*$^{-/-}$ mice, *Ahr*$^{-/-}$ mice show defects in the development of intestinal ILC3s independent of the intestinal microbiota and adaptive immunity. They also lack postnatally "imprinted" CPs and ILFs (8, 9, 38). While AhR regulates the development of intestinal ILC3s in a cell-intrinsic manner (38), it is unlikely to mediate the effects of VIP on the development of intestinal ILC3s. First, SI-LPL ILC3s from *Vip*$^{-/-}$ mice but not *Ahr*$^{-/-}$ mice were fully competent to secrete IL-22. Second, CD4^{+} T cells and CD11c^{+} DC cells were intact in the SI-LPL of *Ahr*$^{-/-}$ mice but markedly reduced in SI-LPL of *Vip*$^{-/-}$ mice.

Our results showing no defect in intestinal ILC3 recruitment in *Vpac2*$^{-/-}$ mice is similar to that reported by Seillet et al. (18). Interestingly, *Vpac2*$^{-/-}$ mice demonstrated a modestly increased susceptibility to *C. rodentium* infection as compared to *Vpac2*$^{-/+}$ mice, accompanied by decreased *Il-22* expression in their small intestines. These data suggest that the in vivo role of VPAC2 may be more important for the activation of intestinal ILC3s by VIP as reported by a recent study (18) but not for their recruitment. Unlike VPAC2, minimal VPAC1 expression was detected on intestinal ILC3s (*SI Appendix*, Fig. S9 *D* and *E*). Despite this finding, *Vpac1*$^{-/-}$ mice and *Vpac1*$^{-/-}$ *Vpac2*$^{-/-}$ mice behaved similarly to *Vip*$^{-/-}$ mice, failing to recruit ILC3s to the small intestines. As a result, both *Vpac1*$^{-/-}$ mice and *Vip*$^{-/-}$ mice were extremely susceptible to *C. rodentium* infection. Thus, it appears that VIP regulates the number of intestinal ILC3s in a manner extrinsic to the ILC3s (i.e., through VPAC1). Our results

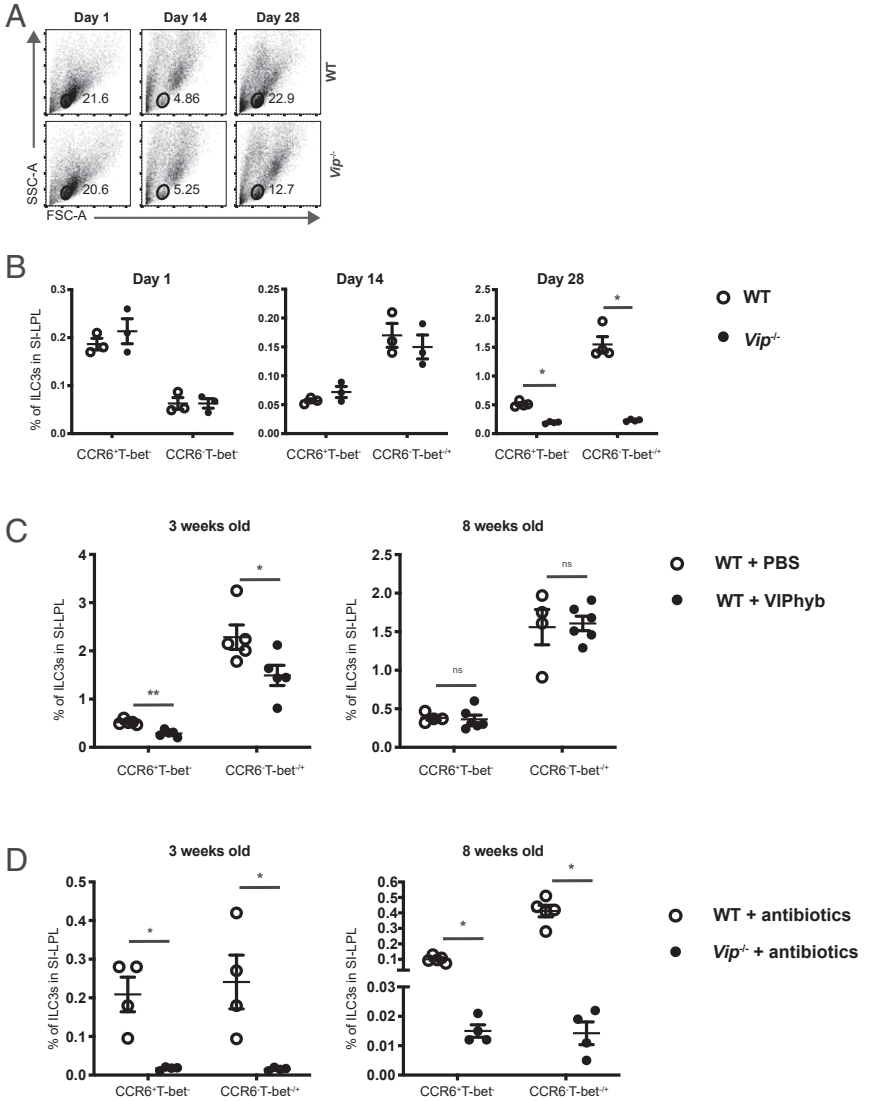

Fig. 7. VIP acts postnatally to induce intestinal ILC3 recruitment independent of the intestinal microbiota. (*A* and *B*) LPLs were isolated from the SI of uninfected WT and *Vip*$^{-/-}$ mice at postnatal day 1, 14, and 28. (*A*) Data are representative fluorescence-activated cell sorting plots showing singlet populations. The percentages of circled populations (lymphocytes) are indicated next to the circles. (*B*) Cells were gated as in *SI Appendix*, Fig. S5*A*. The percentages of ILC3 subsets in SI-LPL of WT and *Vip*$^{-/-}$ mice at indicated ages are presented. Data are representative of two independent experiments. (*C*) PBS or VIPhyb (a VIP antagonist) was injected intraperitoneally into WT mice at the age of 3 wk (*Left*, $n = 5$ for PBS and VIPhyb) or 8 wk (*Right*, $n = 4$ for PBS, $n = 6$ for VIPhyb) for 3 wk followed by the analysis of the percentage of ILC3 subsets in SI-LPL. (*D*) WT and *Vip*$^{-/-}$ mice at the age of 3 wk (*Left*, $n = 4$ for both groups) or 8 wk (*Right*, $n = 5$ for WT, $n = 4$ for *Vip*$^{-/-}$) were treated with antibiotics for 3 wk, followed by the analysis of the percentage of ILC3 subsets in SI-LPL. All data are shown as mean ± SEM $^{*}P < 0.05$, $^{**}P < 0.01$, by Mann–Whitney *U* test.

Downloaded from https://www.pnas.org by 212.129.10.242 on October 30, 2025 from IP address 212.129.10.242.

also show that the VIP–VPAC1 signaling axis controls the recruitment of other intestinal immune cells, such as T cell, B cells, and DCs. Interestingly, the loss of VIP or VPAC1 also leads to impaired immune cell infiltration into the central nervous system (CNS) in experimental autoimmune encephalomyelitis (EAE), a mouse model of multiple sclerosis (54, 55). While it remains unclear whether the migration of immune cells to the small intestine and CNS could share a similar mechanism, *Vpac1*$^{-/-}$ bone marrow–derived hematopoietic cells retain their intrinsic ability to migrate to CNS and induce EAE (55). Since VPAC1 is also expressed by many other cell types, such as myenteric nerve fibers (56), endothelial cells (57), and epithelial cells (58), future studies will involve generating *Vpac1* conditional knockout mouse strains to identify the cell type(s) responsible for VIP-VPAC1 driven recruitment of ILC3 to the intestine.

The absence of a functional VIP–VPAC1 signaling axis led to a generalized defect in the recruitment of immune cells to the small intestine, suggesting that the lack of B cells in *Vip*$^{-/-}$ mice may also contribute to the defective formation of CPs in these mice. It will be interesting to determine whether other cell types (T cell, B cells, and myeloid cells) contribute to the hypersusceptibility of *Vip*$^{-/-}$ and *Vpac1*$^{-/-}$ mice to *C. rodentium* infection. Despite these findings, the loss of VIP–VPAC1 signaling axis appeared to have an exaggerated effect on the ILC3 populations in adult mice (starting as early as the age of week 4). Our results suggest that the reduced numbers of all subsets of DCs, particularly CD103$^+$ DCs, in SI-LPL of *Vip*$^{-/-}$ mice may have led to a further reduction in the recruitment of ILC3s. The marked reduction in CD103$^+$ DCs was associated with decreased RA production by *Vip*$^{-/-}$ mice, as well as lower CCR9 expression by SI-LPL ILC3s. Confirming a key role for RA in inducing CCR9$^+$ gut-homing ILC3s (39), the administration of exogenous RA to *Vip*$^{-/-}$ mice increased the percentage of CCR9$^+$ ILC3s (CCR6$^+$NKp46$^-$). While these findings demonstrate the effect of VIPdeficiency on RA production, this effect is unlikely to occur before birth. Maternal retinoids control PP formation (59), whereas *Vip*$^{-/-}$ mice showed no defect in PP development. Nevertheless, the deficit in RA signaling in either fetal life or after birth controls the numbers and function of ILC3s, leaving the host with heightened susceptibility to infections and chronic inflammatory diseases (59–61). Together, we show that in addition to dietary factors (e.g., AhR ligands and retinoids), VIP serves as an important host factor regulating the number of intestinal ILC3s by maintaining RA production.

Thus, it appears that there are at least two mechanisms through which VIP promotes ILC3 recruitment to the gut. One involves the VIP–VPAC1 mediated migration of ILC3s, while the other involves the maintenance of a population of DC that, through the production of RA, promotes CCR9 expression on ILC3s. This may explain the observations that ILC3 adoptive transfer and RA supplementation into *Vip*$^{-/-}$ mice provides only partial protection against *C. rodentium* infection, since endogenous VIP is missing in both cases. Notably, while our study suggests that the loss of VIP or VPAC1 leads to dramatically reduced ILC3 recruitment to the gut and heightened susceptibility to *C. rodentium* infection, transient depletion of VIP signaling by a chemogenetic approach resulted in increased IL-22 production by ILC3s leading to protection against the same infection (19). It will be very interesting to determine whether long-term depletion of VIP signaling by this chemogenetic technique would reduce ILC3 recruitment to the gut.

In summary, we demonstrate the critical role played by VIP in mediating communication between the ENS and ILC3s. While previous studies have revealed that VIP modulates the intrinsic function of CCR6$^+$ ILC3 through VPAC2 (18, 19), we show that postnatal VIPsignaling promotes the recruitment of ILC3s through extrinsic signaling (i.e., through VPAC1). This VIP–VPAC1–ILC3 signaling axis plays a crucial role in promoting host defense against enteric pathogen infection.

Materials and Methods

Experimental Animals. All mice used in this study were on the B6 genetic background. WT C57BL/6, *Rag1*$^{-/-}$, and *Vpac2*$^{-/-}$ mice were originally purchased from the Jackson laboratory. *Ahr*$^{-/-}$ and *Vpac1*$^{-/-}$ were originally obtained from Saint Antoine Research Center and University of California, respectively. These five mouse strains were then bred in-house at BC Children's Hospital Research Institute (BCCHRI). *Vip*$^{-/-}$ mice were generated as previously described (62) and bred in-house. *Vip*$^{-/-}$ mice were also bred to *Rag1*$^{-/-}$ mice to produce *Rag1*$^{-/-}$*Vip*$^{-/-}$ mice. *Vpac1*$^{-/-}$ mice were bred to *Vpac2*$^{-/-}$ mice to produce *Vpac1*$^{-/-}$*Vpac2*$^{-/-}$ mice. All mice were kept in sterilized, filter-topped cages and fed autoclaved food and water under specific pathogen free conditions. Mice used for experiments were 6 to 12 wk old unless otherwise stated. Male littermates were kept in the same cage (to avoid fighting) during the experiments, whereas female littermates were randomly assigned to experimental groups. All experiments were approved by the University of British Columbia's Animal Care Committee and in direct accordance with the Canadian Council on Animal Care guidelines.

Bacterial Strains and Infection of Mice. *C. rodentium* DBS100 (streptomycin-sensitive) (25), a streptomycin-resistant derivative of DBS100 (Cr) (26), or a luminescence-expressing *C. rodentium* strain (Cr-lux, also Strep^R) was cultured in Luria Broth in a shaker (200 rpm) at 37 °C overnight. To generate the Cr-lux strain, a *Photorhabdus luminescens* lux operon was cloned downstream of a PLtetO promoter (63, 64) and introduced onto the chromosome of Cr as previously described (65). Mice were orally gavaged with 0.1 mL of an undiluted or diluted overnight bacterial culture, and each mouse received $5.0 \times 10^6 \sim 2.5 \times 10^8$ colony-forming units of bacteria. The infection lasted for 5 to 10 d, and the colonization levels of Cr and Cr-lux strains in mice were comparable.

Data Availability. All study data are included in the article and/or *SI Appendix*.

ACKNOWLEDGMENTS. We thank BCCHRI staff for assistance with mouse experiments, L. Xu from the flow core facility for assistance with cell sorting, C. Dai for assistance with tail vein injection, R. Dyer in the Analytical Core for Metabolomics and Nutrition for assistance with vitamin A analysis, T. Huang for assistance with immunostaining, and M. Kuan and N. Moore for assistance with mRNA work. We also thank Genentech for providing rIL-22. This work was supported by grants from the National Sciences and Engineering Research Council to K.J. and Crohn's and Colitis Canada to K.J. and B.A.V. F.A.G. was supported by a Four-Year Doctoral Fellowship from the University of British Columbia. E.S.B. was supported by a studentship from BCCHRI. B.A.V. is the Children with Intestinal and Liver Disorders (CH.I.L.D) Foundation Chair in Pediatric Gastroenterology. K.J. is a Senior Clinician Scientist supported by the BCCHR Clinician Scientists Award Program, University of British Columbia, and the CH.I.L.D Foundation.

1. M. Colonna, Innate lymphoid cells: Diversity, plasticity, and unique functions in immunity. *Immunity* **48**, 1104–1117 (2018).
2. A. N. J. McKenzie, H. Spits, G. Eberl, Innate lymphoid cells in inflammation and immunity. *Immunity* **41**, 366–374 (2014).
3. D. J. Silberger, C. L. Zindl, C. T. Weaver, Citrobacter rodentium: A model enteropathogen for understanding the interplay of innate and adaptive components of type 3 immunity. *Mucosal Immunol.* **10**, 1108–1117 (2017).
4. G. F. Sonnenberg, D. Artis, Innate lymphoid cells in the initiation, regulation and resolution of inflammation. *Nat. Med.* **21**, 698–708 (2015).
5. J. Emgård *et al.*, Oxysterol sensing through the eeceptor GPR183 promotes the lymphoid-tissue-inducing function of innate lymphoid cells and colonic inflammation. *Immunity* **48**, 120–132.e8 (2018).
6. T. Willinger, Metabolic control of innate lymphoid cell migration. *Front. Immunol.* **10**, 2010 (2019).
7. C. S. Klose *et al.*, A T-bet gradient controls the fate and function of CCR6-RORγt+ innate lymphoid cells. *Nature* **494**, 261–265 (2013).
8. J. S. Lee *et al.*, AHR drives the development of gut ILC22 cells and postnatal lymphoid tissues via pathways dependent on and independent of Notch. *Nat. Immunol.* **13**, 144–151 (2011).
9. E. A. Kiss *et al.*, Natural aryl hydrocarbon receptor ligands control organogenesis of intestinal lymphoid follicles. *Science* **334**, 1561–1565 (2011).
10. A. Mortha, K. Burrows, Cytokine networks between innate lymphoid cells and myeloid cells. *Front. Immunol.* **9**, 191 (2018).
11. A. Wallrapp *et al.*, The neuropeptide NMU amplifies ILC2-driven allergic lung inflammation. *Nature* **549**, 351–356 (2017).
12. H. Veiga-Fernandes, D. Artis, Neuronal-immune system cross-talk in homeostasis. *Science* **359**, 1465–1466 (2018).
13. C. S. N. Klose *et al.*, The neuropeptide neuromedin U stimulates innate lymphoid cells and type 2 inflammation. *Nature* **549**, 282–286 (2017).

Downloaded from https://www.pnas.org by 212.129.10.242 on October 30, 2025 from IP address 212.129.10.242.

14. J. Dalli, R. A. Colas, H. Arnardottir, C. N. Serhan, Vagal regulation of group 3 innate lymphoid cells and the immunoresolvent PCTR1 controls infection resolution. *Immunity* **46**, 92–105 (2017).
15. V. Cardoso *et al*., Neuronal regulation of type 2 innate lymphoid cells via neuromedin U. *Nature* **549**, 277–281 (2017).
16. M. Delgado, D. Ganea, Vasoactive intestinal peptide: A neuropeptide with pleiotropic immune functions. *Amino Acids* **45**, 25–39 (2013).
17. C. Abad *et al*., VIP in inflammatory bowel disease: State of the art. *Endocr. Metab. Immune Disord. Drug Targets* **12**, 316–322 (2012).
18. C. Seillet *et al*., The neuropeptide VIP confers anticipatory mucosal immunity by regulating ILC3 activity. *Nat. Immunol.* **21**, 168–177 (2020).
19. J. Talbot *et al*., Feeding-dependent VIP neuron-ILC3 circuit regulates the intestinal barrier. *Nature* **579**, 575–580 (2020).
20. R. G. Domingues, M. R. Hepworth, Immunoregulatory sensory circuits in group 3 innate lymphoid cell (ILC3) function and tissue homeostasis. *Front. Immunol.* **11**, 116 (2020).
21. V. S. Conlin *et al*., Vasoactive intestinal peptide ameliorates intestinal barrier disruption associated with Citrobacter rodentium-induced colitis. *Am. J. Physiol. Gastrointest. Liver Physiol.* **297**, G735–G750 (2009).
22. V. Morampudi *et al*., Vasoactive intestinal peptide prevents PKCε-induced intestinal epithelial barrier disruption during EPEC infection. *Am. J. Physiol. Gastrointest. Liver Physiol.* **308**, G389–G402 (2015).
23. X. Guo *et al*., Induction of innate lymphoid cell-derived interleukin-22 by the transcription factor STAT3 mediates protection against intestinal infection. *Immunity* **40**, 25–39 (2014).
24. X. Guo *et al*., Innate lymphoid cells control early colonization resistance against intestinal pathogens through ID2-dependent regulation of the microbiota. *Immunity* **42**, 731–743 (2015).
25. D. B. Schauer, S. Falkow, Attaching and effacing locus of a Citrobacter freundii biotype that causes transmissible murine colonic hyperplasia. *Infect. Immun.* **61**, 2486–2492 (1993).
26. K. S. Bergstrom *et al*., Muc2 protects against lethal infectious colitis by disassociating pathogenic and commensal bacteria from the colonic mucosa. *PLoS Pathog.* **6**, e1000902 (2010).
27. W. Deng, B. A. Vallance, Y. Li, J. L. Puente, B. B. Finlay, Citrobacter rodentium translocated intimin receptor (Tir) is an essential virulence factor needed for actin condensation, intestinal colonization and colonic hyperplasia in mice. *Mol. Microbiol.* **48**, 95–115 (2003).
28. M. M. Curtis *et al*., The gut commensal Bacteroides thetaiotaomicron exacerbates enteric infection through modification of the metabolic landscape. *Cell Host Microbe* **16**, 759–769 (2014).
29. Y. Zheng *et al*., Interleukin-22 mediates early host defense against attaching and effacing bacterial pathogens. *Nat. Med.* **14**, 282–289 (2008).
30. R. Basu *et al*., Th22 cells are an important source of IL-22 for host protection against enteropathogenic bacteria. *Immunity* **37**, 1061–1075 (2012).
31. G. F. Sonnenberg, L. A. Monticelli, M. M. Elloso, L. A. Fouser, D. Artis, CD4(+) lymphoid tissue-inducer cells promote innate immunity in the gut. *Immunity* **34**, 122–134 (2011).
32. S. M. Dann *et al*., IL-17A promotes protective IgA responses and expression of other potential effectors against the lumen-dwelling enteric parasite Giardia. *Exp. Parasitol.* **156**, 68–78 (2015).
33. T. A. Pham *et al*.; Sanger Mouse Genetics Project, Epithelial IL-22RA1-mediated fucosylation promotes intestinal colonization resistance to an opportunistic pathogen. *Cell Host Microbe* **16**, 504–516 (2014).
34. Y. Goto *et al*., Innate lymphoid cells regulate intestinal epithelial cell glycosylation. *Science* **345**, 1254009 (2014).
35. O. B. Parks, D. A. Pociask, Z. Hodzic, J. K. Kolls, M. Good, Interleukin-22 Signaling in the Regulation of intestinal health and disease. *Front. Cell Dev. Biol.* **3**, 85 (2016).
36. C. A. Lindemans *et al*., Interleukin-22 promotes intestinal-stem-cell-mediated epithelial regeneration. *Nature* **528**, 560–564 (2015).
37. X. Wu *et al*., Vasoactive intestinal polypeptide promotes intestinal barrier homeostasis and protection against colitis in mice. *PLoS One* **10**, e0125225 (2015).
38. J. Qiu *et al*., The aryl hydrocarbon receptor regulates gut immunity through modulation of innate lymphoid cells. *Immunity* **36**, 92–104 (2012).
39. M. H. Kim, E. J. Taparowsky, C. H. Kim, Retinoic acid differentially regulates the migration of innate lymphoid cell subsets to the gut. *Immunity* **43**, 107–119 (2015).
40. C. H. Kim, S. Hashimoto-Hill, M. Kim, Migration and tissue tropism of innate lymphoid cells. *Trends Immunol.* **37**, 68–79 (2016).
41. E. C. Mackley *et al*., CCR7-dependent trafficking of RORγ$^+$ ILCs creates a unique microenvironment within mucosal draining lymph nodes. *Nat. Commun.* **6**, 5862 (2015).
42. M. Iwata *et al*., Retinoic acid imprints gut-homing specificity on T cells. *Immunity* **21**, 527–538 (2004).
43. M. Svensson *et al*., CCL25 mediates the localization of recently activated CD8alphabeta(+) lymphocytes to the small-intestinal mucosa. *J. Clin. Invest.* **110**, 1113–1121 (2002).
44. D. J. Campbell, E. C. Butcher, Intestinal attraction: CCL25 functions in effector lymphocyte recruitment to the small intestine. *J. Clin. Invest.* **110**, 1079–1081 (2002).
45. E. Jaensson-Gyllenbäck *et al*., Bile retinoids imprint intestinal CD103+ dendritic cells with the ability to generate gut-tropic T cells. *Mucosal Immunol.* **4**, 438–447 (2011).
46. T. Aychek *et al*., IL-23-mediated mononuclear phagocyte crosstalk protects mice from *Citrobacter rodentium*-induced colon immunopathology. *Nat. Commun.* **6**, 6525 (2015).
47. G. F. Sonnenberg, L. A. Fouser, D. Artis, Border patrol: Regulation of immunity, inflammation and tissue homeostasis at barrier surfaces by IL-22. *Nat. Immunol.* **12**, 383–390 (2011).
48. R. Blomhoff, H. K. Blomhoff, Overview of retinoid metabolism and function. *J. Neurobiol.* **66**, 606–630 (2006).
49. A. Habtezion, L. P. Nguyen, H. Hadeiba, E. C. Butcher, Leukocyte trafficking to the small intestine and colon. *Gastroenterology* **150**, 340–354 (2016).
50. J. M. Li *et al*., Modulation of immune checkpoints and graft-versus-leukemia in allogeneic transplants by antagonizing vasoactive intestinal peptide signaling. *Cancer Res.* **76**, 6802–6815 (2016).
51. T. W. Moody *et al*., A vasoactive intestinal peptide antagonist inhibits non-small cell lung cancer growth. *Proc. Natl. Acad. Sci. U.S.A.* **90**, 4345–4349 (1993).
52. Z. Al Nabhani *et al*., A weaning reaction to microbiota is required for resistance to immunopathologies in the adult. *Immunity* **50**, 1276–1288.e5 (2019).
53. D. R. Withers, M. R. Hepworth, Group 3 innate lymphoid cells: Communications hubs of the intestinal immune system. *Front. Immunol.* **8**, 1298 (2017).
54. C. Abad *et al*., Vasoactive intestinal peptide loss leads to impaired CNS parenchymal T-cell infiltration and resistance to experimental autoimmune encephalomyelitis. *Proc. Natl. Acad. Sci. U.S.A.* **107**, 19555–19560 (2010).
55. C. Abad *et al*., VPAC1 receptor (Vipr1)-deficient mice exhibit ameliorated experimental autoimmune encephalomyelitis, with specific deficits in the effector stage. *J. Neuroinflammation* **13**, 169 (2016).
56. S. Schulz *et al*., Immunocytochemical identification of VPAC1, VPAC2, and PAC1 receptors in normal and neoplastic human tissues with subtype-specific antibodies. *Clin. Cancer Res.* **10**, 8235–8242 (2004).
57. S. Grant, E. M. Lutz, A. R. McPhaden, R. M. Wadsworth, Location and function of VPAC1, VPAC2 and NPR-C receptors in VIP-induced vasodilation of porcine basilar arteries. *J. Cereb. Blood Flow Metab.* **26**, 58–67 (2006).
58. D. Jayawardena *et al*., Expression and localization of VPAC1, the major receptor of vasoactive intestinal peptide along the length of the intestine. *Am. J. Physiol. Gastrointest. Liver Physiol.* **313**, G16–G25 (2017).
59. S. A. van de Pavert *et al*., Maternal retinoids control type 3 innate lymphoid cells and set the offspring immunity. *Nature* **508**, 123–127 (2014).
60. S. P. Spencer *et al*., Adaptation of innate lymphoid cells to a micronutrient deficiency promotes type 2 barrier immunity. *Science* **343**, 432–437 (2014).
61. L. A. Mielke *et al*., Retinoic acid expression associates with enhanced IL-22 production by γδ T cells and innate lymphoid cells and attenuation of intestinal inflammation. *J. Exp. Med.* **210**, 1117–1124 (2013).
62. V. Lelievre *et al*., Gastrointestinal dysfunction in mice with a targeted mutation in the gene encoding vasoactive intestinal polypeptide: A model for the study of intestinal ileus and Hirschsprung's disease. *Peptides* **28**, 1688–1699 (2007).
63. R. Lutz, H. Bujard, Independent and tight regulation of transcriptional units in *Escherichia coli* via the LacR/O, the TetR/O and AraC/I1-I2 regulatory elements. *Nucleic Acids Res.* **25**, 1203–1210 (1997).
64. G. M. Robinson, K. M. Tonks, R. M. Thorn, D. M. Reynolds, Application of bacterial bioluminescence to assess the efficacy of fast-acting biocides. *Antimicrob. Agents Chemother.* **55**, 5214–5220 (2011).
65. H. P. Sham *et al*., Attaching and effacing bacterial effector NleC suppresses epithelial inflammatory responses by inhibiting NF-κB and p38 mitogen-activated protein kinase activation. *Infect. Immun.* **79**, 3552–3562 (2011).

Downloaded from https://www.pnas.org by 212.129.10.242 on October 30, 2025 from IP address 212.129.10.242.